Compressive properties of thin tow-based discontinuous composites

Composites Part B 292 (2025) 112085

Contents lists available at ScienceDirect

Composites Part B

journal homepage: www.elsevier.com/locate/compositesb

Compressive properties of thin tow-based discontinuous composites

Ioannis Katsivalis [a,b,*], Aree Tongloet [c], Xun Wu [c,g], Monica Norrby [d], Florence Moreau [e], Soraia Pimenta [f], Michael R. Wisnom [c], Dan Zenkert [d], Leif E. Asp [a]

[a] Department of Industrial and Materials Science, Chalmers University of Technology, Sweden
[b] Department of Architecture & Civil Engineering, University of Bath, UK
[c] Bristol Composites Institute, University of Bristol, UK
[d] Department of Engineering Mechanics, KTH, Sweden
[e] Oxeon AB, Sweden
[f] Department of Mechanical Engineering, Imperial College London, UK
[g] Faculty of Engineering and Physical Sciences, University of Southampton, UK

ARTICLE INFO

Handling Editor: Prof. Ole Thomsen

Keywords:
Tow-based discontinuous composites
Compressive testing
Sandwich beam bending
Damage characterisation
Fractography

ABSTRACT

Ultra-thin tow-based discontinuous composites are an emerging class of composite materials which can be used for high performance applications in a wide range of industries. They offer significant advantages compared to continuous composites, such as reduced waste material, enhanced formability and even increased mechanical properties. However, the properties of composite materials under compression are often a limiting factor in structural design. Measuring the compressive properties of composites is also non-trivial, as premature failures are occurring often with the existing testing standards. Finally, the compressive response of discontinuous composites is currently unclear as the existing studies are limited. This work presents a full experimental campaign on the characterization of the compressive response of ultra-thin tow-based discontinuous composites. A uniaxial test is initially employed which reveals instabilities, premature failures and large experimental scatter. Afterwards, a sandwich beam bending test is employed which allows to measure the compressive properties accurately with low variability. The compressive strains measured exceed 1 %, which is also the tensile limit for this material. The agreement between the tensile and compressive strength was investigated by using scanning electron microscopy which revealed that the damage was controlled by matrix deformation in the tow interfaces.

1. Introduction

Tow-Based Discontinuous Composites (TBDCs) are a new and emerging class of composite materials [1–4]. TBDCs are bio-inspired, mimicking materials found in nature such as nacre [5]. Utilising the Brick-and-Mortar (BaM) architecture of nacre and other similar materials [6], TBDCs can achieve excellent mechanical properties, which are directly comparable to continuous composites [7,8], while also minimising the scrap and waste material and allowing to achieve complex shapes due to the enhanced forming capabilities. In addition, the random tape distribution of TBDCs allows to achieve in-plane isotropy while the use of ultra-thin tapes increases their mechanical properties by suppressing transverse cracking and delamination. This delays tape pull-out to higher strain levels [7,9,10].

The compressive strength of Carbon Fibre Reinforced Polymers (CFRPs) is a critical design parameter in high-performance applications. Typically, the compressive strength of unidirectional continuous CFRPs is lower compared to their tensile strength as the failure is governed by the matrix [11]. In addition, the compressive strength of continuous CFRPs is governed by instabilities across different scales. At a micro level, fibres may fail due to the instability of the graphite crystallites [12] while at a meso level, instabilities lead to micro-buckling and kinking [13]. Finally at a macro level the instabilities can lead to global buckling of the specimen. It is worth noting that these levels are interconnected and instabilities at fibre level can lead to kink bands which is a common global damage mechanism. These instabilities can be triggered due to material and geometrical non-linearities [14].

In addition, these instabilities can be exacerbated by standard compressive testing methods. Uniaxial compressive tests (such as ASTM D3410 [15]) utilise long end tabs and short gauge lengths to minimise instabilities. However, there is also a strong interaction between shear and compression [16] and the high stress concentrations in the gripping

* Corresponding author. Department of Industrial and Materials Science, Chalmers University of Technology, Sweden.
E-mail address: ioannis.katsivalis@chalmers.se (I. Katsivalis).

https://doi.org/10.1016/j.compositesb.2024.112085
Received 13 September 2024; Received in revised form 25 November 2024; Accepted 17 December 2024
Available online 17 December 2024

areas [17] can lead to premature failures. A different approach to measuring the compressive properties of CFRPs is the use of flexural bending tests. Flexural tests avoid specimen misalignments and high stress concentrations at the loading points. In addition, pin-ended buckling tests can completely eliminate stress concentrations, produce consistently high compressive strains but require more complex experimental setups [18]. However, the strain gradient through the thickness of the bending specimens inhibits the compressive damage and can exaggerate the apparent compressive properties of CFRPs.

Yokozeki et al. [19] evaluated the non-linear compressive properties of unidirectional CFRPs using a modified sandwich beam specimen under flexure and the authors achieved a 31 % percent increase of the compressive strength when compared to coupon based uniaxial strength measurements [20]. Recently, Wu and Wisnom [21] developed a four-point Sandwich Beam Bending (SBB) specimen which was used to accurately measure the compressive strain of unidirectional CFRP specimens. The test method was based on ASTM D5467 [22] and led to consistent compressive failure in the gauge section with low experimental scatter. The authors also demonstrated that, for sufficiently thick beams, the strain gradient effect was minimal.

Feraboli et al. [23] evaluated the compressive properties of TBDCs made from thick tapes (0.125 mm). The authors reported an elastic modulus in the region of 45–55 GPa with high experimental scatter while the compressive strength achieved was about 250 MPa. It is worth noting that the modulus was similar in tension and compression but the strength under compression was higher. A similar trend was reported by Selezneva and Lessard [24] who also used thick tapes (0.140 mm) for the TBDCs manufactured. Martulli et al. [25] also performed uniaxial compressive testing on SMC-based TBDC specimens (0.115 mm tow thickness) and observed higher strength under compression than tension. However, in these studies the strength under both tension and compression is significantly lower (below 300 MPa) than in conventional continuous Quasi-Isotropic (QI) laminates.

It was demonstrated in the past that the tensile strength of ultra-thin TBDCs can outperform conventional QI composites and reach values above 650 MPa [7]. The higher strengths reached in that study were related to the use of ultra-thin tapes for the manufacturing of the TBDCs and the damage was caused by tape pull-out and was controlled by the shear deformation of the matrix. It is hypothesised that, due to the complex micro-architecture of the ultra-thin TBDCs, their compressive failure will also be governed by the resin fracture mechanism at the tow interfaces. This is motivated by the potential suppression of fibre micro-buckling in the material, inherent to the minimal fibre undulation and limited through-thickness extension of any fibre misaligned “defect zone” in the material [26]. Therefore, it is also hypothesised that the compressive strength of the ultra-thin TBDCs may be closer to their tensile strength. However, a study on the compressive properties of high strength, ultra-thin TBDCs is currently lacking.

This paper explores for the first time the compressive properties of ultra-thin TBDCs by performing two different sets of tests. The first test was based on uniaxial compression following ASTM D3410 while the second one was based on the sandwich beam bending method proposed by Wu and Wisnom [21]. In addition, two different geometries for the sandwich beam bending test were considered. The two different sets of tests revealed the effect of instabilities and highlighted the importance of the test method in obtaining consistent and repeatable results. The damage and fracture were characterised using optical microscopy and fractography while the experimental results were validated by comparing with analytical methods. The measurements from the sandwich beam bending test revealed strains exceeding 1 % thus highlighting the high-performance potential of ultra-thin TBDCs. This is the first time that the compressive properties of ultra-thin TBDCs were measured, and the presented results exceed overwhelmingly other values reported in the literature for discontinuous composites. These findings highlight the potential of using ultra-thin TBDCs in high-performance applications.

2. Methodology

2.1. Plate manufacturing

Two ultra-thin TBDC panels were manufactured for the two types of compressive tests. Details of the panel manufacturing can be found in earlier publications by the authors [7,8] but a summary is also provided here. The panels had dimensions 300 × 300 mm and their thickness was 1 mm. The PyrofilTM MR70 12 P carbon fibre from Mitsubishi Chemical Carbon Fiber and Composites was used for the TeXtreme tapes which were manufactured by Oxeon AB with their spread tow technology. This resulted in ultra-thin tapes with dimensions 40 mm (length) x 20 mm (width) and a nominal thickness of 21.4 μm. An automated tape placement method was utilised to ensure the random orientation and position of each tape which was critical in to ensure the quasi-isotropic response of the specimens. Once the preforms were made, they were then cured at high pressures (20 bar) with press moulding. It is worth noting that before the random placement, the tapes were partially impregnated which combined with the high moulding pressure allowed to minimise the resin pockets, increase the fibre volume fraction, and achieve higher mechanical properties. Fig. 1 shows a characteristic panel and a cross-section of the ultra-thin TBDC material.

2.2. Uniaxial testing

The uniaxial compressive testing followed the guidelines of ASTM D3410 [15] and utilised the IITRI Compression Test Fixture. The specimen dimensions were 140 × 10 mm while the end tabs were 65 mm long on each side, leaving a 10 mm long test area. The dimensions of the end tabs were determined to keep the gauge length short enough to prevent Euler buckling. For strain measurements, a stereo DIC system on the front side of the specimen. The use of two cameras allows to resolve out-of-plane displacements and could therefore identify buckling. A total of six specimens were tested at a universal loading machine with a load cell of 100 kN. The speed of the test was 0.6 mm/min which led to specimen failure within 5–10 min. Fig. 2 shows a sketch of the specimens and a characteristic specimen before testing.

2.3. Sandwich beam bending (SBB) testing

The SBB testing followed the design guidelines found in Ref. [21] and was also based on ASTM D5467 [22]. Due to TBDC panel manufacturing limitation, the maximum length of the SBB specimen was 300 mm. Therefore, the first design of the SBB (referred as short SBB from now on) can be seen in Fig. 3a. The SBB specimen consists of the TBDC top skin (1 mm thick), a PMMA core (18 mm thick), and a UD IM7/8552 carbon/epoxy bottom skin (1 mm thick). It is worth noting that in the past, the authors used a wood core for similar tests. However, wood displayed variability, and some specimens failed due to splitting in the core. Therefore, the PMMA material was selected as it was easier to obtain in the required dimensions without the additional requirement for machining. The width of all specimens was 15 mm. The three layers of the SBB specimen were adhesively bonded with Araldite 2022–1 [27]. Before bonding, the PMMA was sandblasted, and the composite surfaces were sanded. Finally, all surfaces were degreased using isopropanol. Uniform pressure was applied during the curing of the adhesive to ensure thin and uniform thickness in the bondlines.

The specimens tested in Ref. [21] were significantly longer (450–1250 mm) which allowed to reduce the shear stresses in the core. Therefore, to minimise shear in the core, it was decided to develop a second design for the SBB specimen, which uses a longer support span. To manufacture these specimens, TBDC extension skins were used, which were adhesively bonded to the ends of the main top skin. Patches were also used to ensure proper stress transfer between the main top skin and the extensions. This longer span increases the ratio between the maximum stresses in the skins and those in the core, without affecting

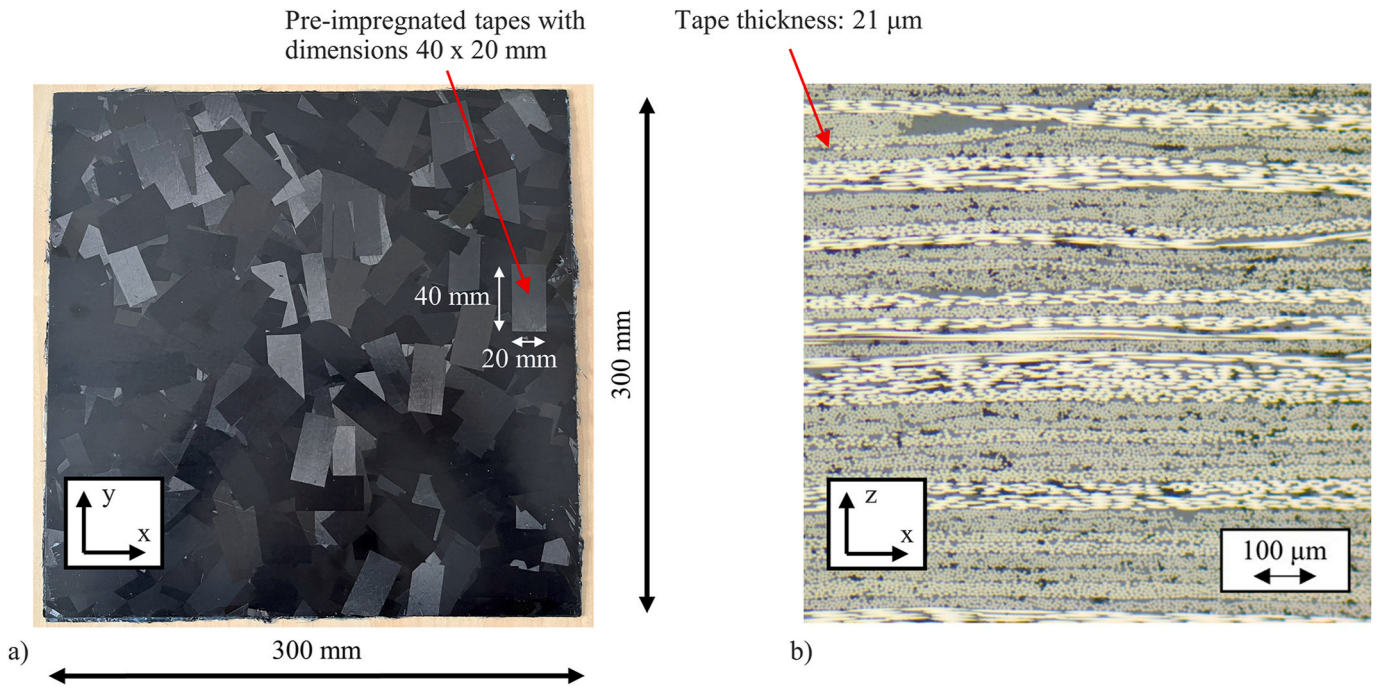

Fig. 1. a) Typical manufactured ultra-thin TBDC panel and b) characteristic cross-section showing the complex micro-architecture.

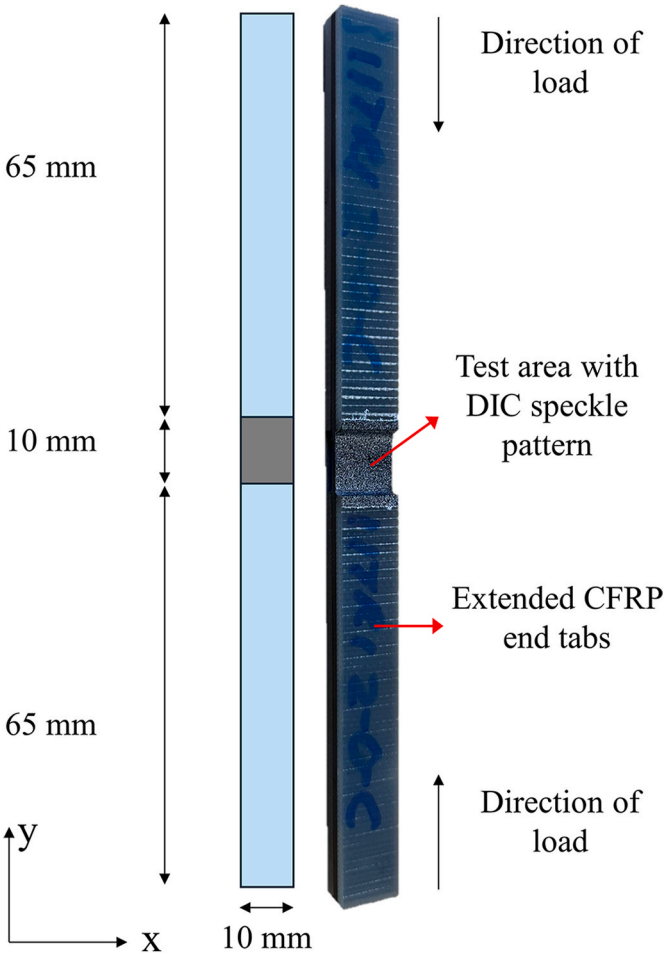

Fig. 2. Uniaxial compressive testing specimen geometry.

the accuracy of measured compressive strains in the TBDC skins within the loading pins. The detailed design of the second SBB specimens can be found in Fig. 3b.

The load span was 40 mm, the load was applied with 25 mm diameter loading noses at a constant rate of 2 mm/min. Rubber pads were used to avoid hard contact between the loading noses and the top skin of the SBB specimens. A universal loading machine was used for the testing and the load-displacement curves were recorded. Finally, Vishay linear strain gauges were positioned in the central parts of the top and bottom skins to capture the tensile and compressive strains. A minimum of five specimens were tested for each configuration and Fig. 4 shows the experimental setup. Table 1 shows the material properties of the SBB specimens which were used for the analytical strain calculations and the specimen design.

2.4. SEM analysis

SEM analysis was used to characterise the damage of the SBB specimens. Characteristic surfaces were obtained from the SBB specimens after failure. The specimens, with approximate dimensions 10 × 10 mm, were extracted by opening delaminated specimens post fracture and ensuring that no damage was introduced during the handling of the specimens. All surfaces examined were found in the central parts of the specimens (between the loading noses) and close to the locations of fracture. The specimens were coated with a thin layer of gold and a JEOL 7800 F prime was used for the SEM analysis. The acceleration voltage was 5 kV and the magnification levels were ranging between ×100 and x5000.

3. Results

3.1. Uniaxial testing

Fig. 5a shows the full-field out-of-plane displacement and Fig. 5b shows the in-plane longitudinal strain evolution with increasing load in one of the tested specimens. Resolving the full-field strain was rather complex due to the limited space and the size of the testing fixture. Therefore, the quality of the DIC images was poor for some specimens.

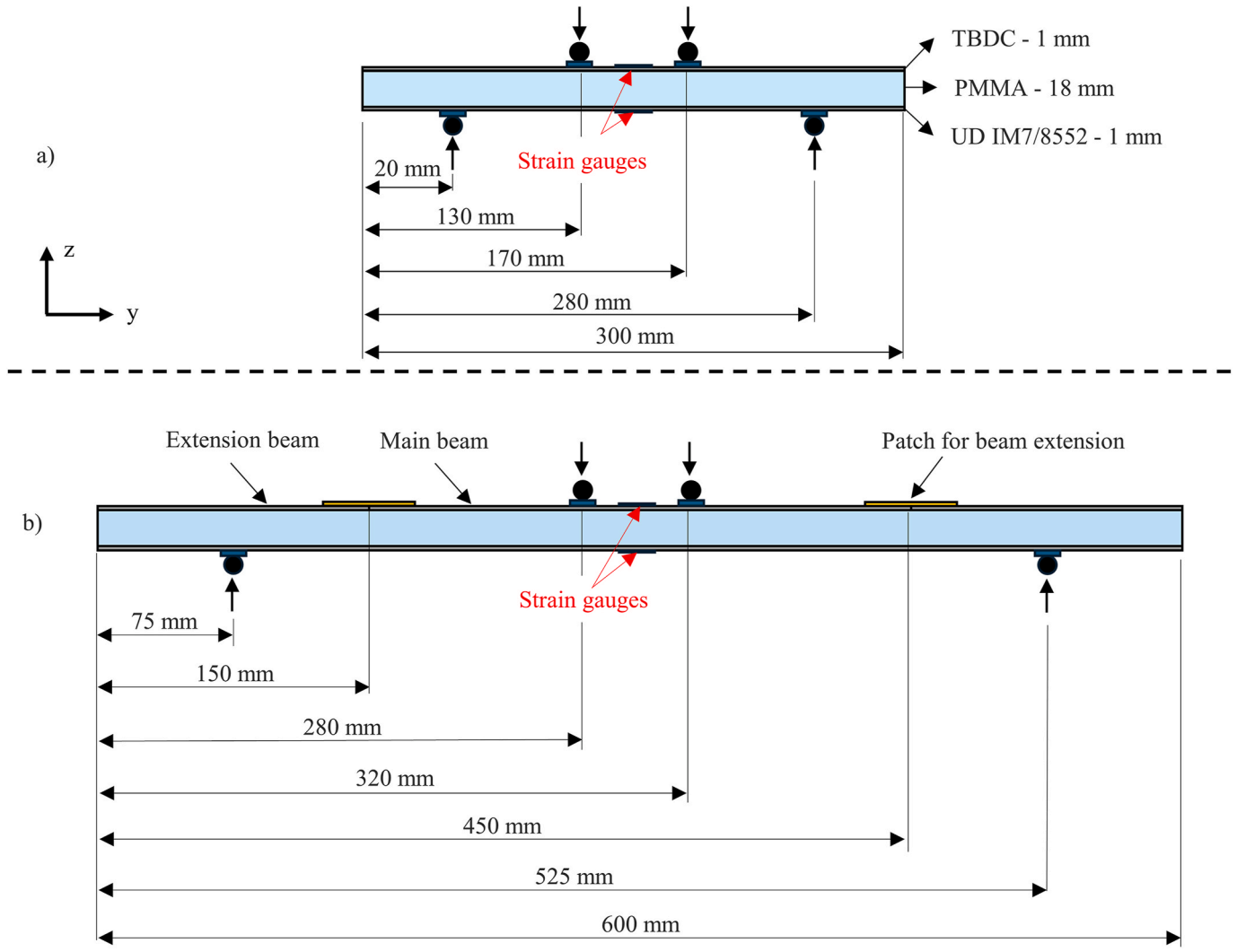

Fig. 3. SBB specimen geometry for the a) short and b) long configuration (not to scale).

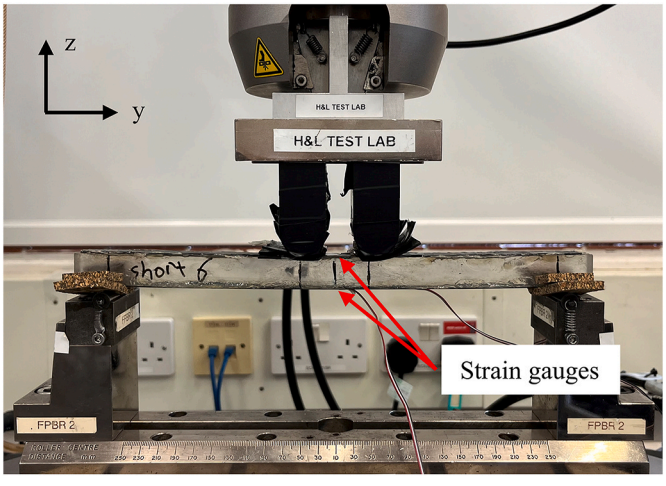

Fig. 4. Experimental setup for the SBB testing (short SBB configuration shown).

However, the DIC analysis could still reveal significant out-of-plane displacement and rotation in the specimens. This was not only highlighted by the magnitude of the out-of-plane displacements but also by the non-uniform in-plane strain fields in the loading direction caused by bending.

Table 1
Material properties for the SBB specimens.

Material	Longitudinal modulus (GPa)
TBDC [7]	70
UD IM7/8552 [28]	164
PMMA [29]	3.2

Fig. 6a shows the stress-strain response for all six specimens tested. The stress was calculated by dividing the force over the area of the cross-section of each specimen while digital linear extensometers were used in the central parts of the specimens to extract the compressive strain. The red line in Fig. 6a corresponds to the tensile stiffness (70 GPa) of the TBDC specimens as obtained by tensile testing [7]. In addition, Fig. 6b performs a bending check by pointing out the specimens for which the strain deviated by more than 10 % from the theoretical value. It is evident from Fig. 6a and b that three specimens have an approximately linear response and good agreement with the tensile stiffness while three specimens develop a strongly non-linear response, which is a clear indication of material eccentricity leading to bending and premature failures. For the specimens with the stiff response, some slight non-linearities can be observed before final failure. The other three specimens with the highly non-linear response were excluded from the analysis. The variability in the experimental results is related to the

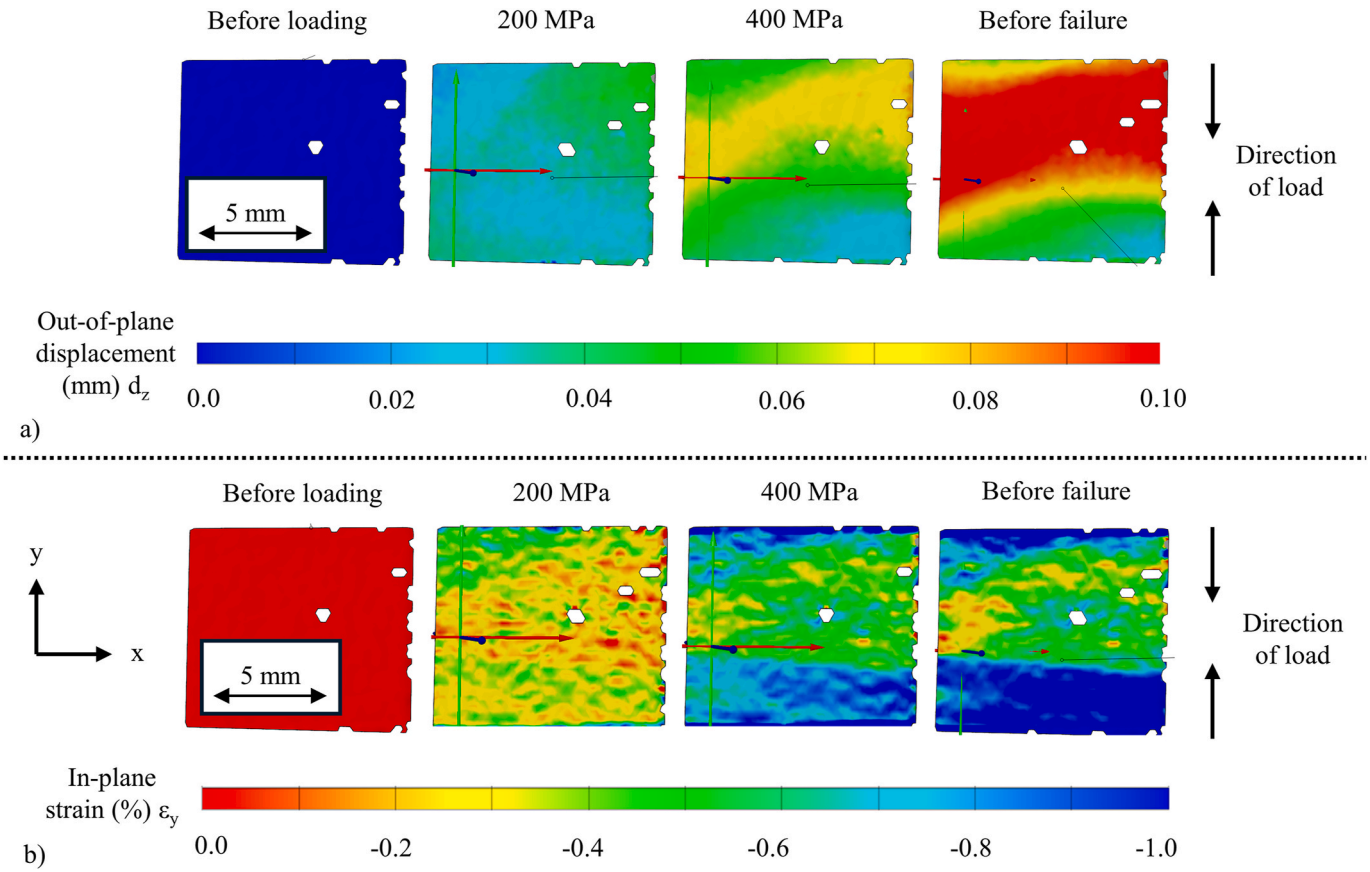

Fig. 5. Full-field a) out-of-plane displacement and b) in-plane longitudinal strain distribution in a characteristic uniaxial testing specimen with increasing load. The x direction is the in-plane direction along the width, while the y direction is the in-plane direction along the length (loading direction).

sensitivity of the test setup to instabilities (for instance due to small variation in the thickness of the specimens) and the nature of TBDC materials which have more scatter than typical laminates due to the random tape orientation. Table 2 summarises the experimental results from the uniaxial testing and compares them with the tensile properties obtained in Ref. [7].

It is worth noting that the compressive stiffness is comparable to the tensile stiffness while the strength and strain to failure reached about 80 % of the tensile response. However, careful analysis of the DIC data and visual inspection of the failed specimens suggest that all specimens suffered from premature failures. For instance, Fig. 7 shows a characteristic specimen after failure. The local compressive failure led to delamination which created a "macroscopic kink band" (with kinking at the tape scale) and the evident misalignment in the specimen. It was not possible to obtain fracture surfaces from the internal tapes of the specimen without causing further damage to the specimens and therefore SEM analysis was not conducted. The experimental results from the uniaxial testing show that the full compressive strength was not reached and justify the development of the second set of tests using the SBB specimens.

3.2. Sandwich beam bending testing

Fig. 8 plots the load-strain response of the short and long SBB specimens. The strain gauge of the top skin measures the compressive strain in the TBDC (negative strains in Fig. 8) while the strain gauge on the bottom skin measures the tensile strain the UD composite (positive strains in Fig. 8). The bottom skin measurement is used to validate that the sandwich beam works as designed. In addition, the response of the sandwich beam was predicted analytically (using simple beam theory for sandwich structures) based on the material properties found in Table 1. The analytical predictions were initially used to design the specimen geometry and later to validate the specimen response during testing. These analytical predictions are also included in Fig. 8.

The tensile strain for both the short and long specimens followed a linear response while the compressive strain in the TBDC skin displayed some non-linearities (consistent with compressive loading), especially for the short configuration which also led to higher loads. These non-linearities were not predicted by the analytical solution [30] which assumed perfectly elastic behaviour for all materials.

All specimens failed in the gauge section due to compressive failure and the compressive strains recorded in the TBDC top skin were significantly higher compared to the strains recorded during uniaxial compressive testing. Table 3 summarises the compressive strains measured. The short SBB specimens achieved slightly higher strains compared to the long ones, but the differences were within the experimental scatter. The compressive strains achieved, reached and even exceeded in some cases the tensile strain-to-failure of the ultra-thin TBDCs.

In addition, the compressive strains reached with the SBB specimens exceeded by about 20 % the compressive strains recorded during uniaxial testing. Similar increases in compressive strength of unidirectional CFRPs have been reported by other authors who have tested both under uniaxial and flexural compression, e.g. Ref. [19]. Higher results are sometimes obtained in bending due to the strain gradient, which was avoided in the present tests by using a 20 mm deep sandwich specimen. It is worth noting that, with the current setup, the compressive stress cannot be measured directly. However, the strength was estimated assuming that the elastic modulus of the TBDC material is equal under tension and compression. This assumption is motivated by the observations made during the uniaxial compressive testing.

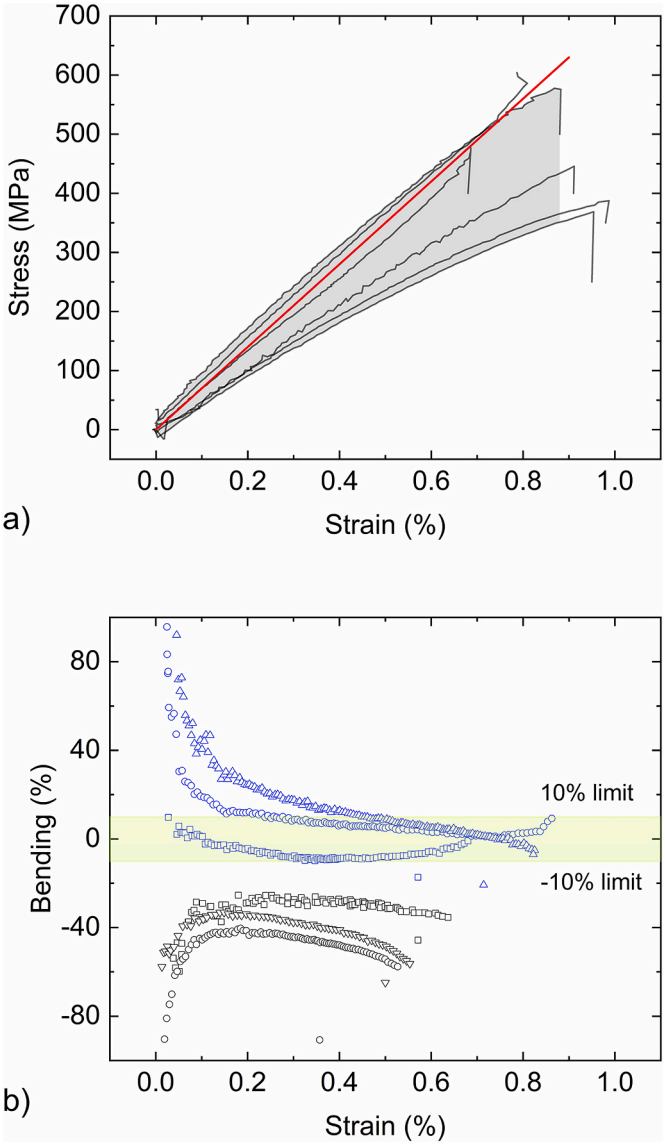

Fig. 6. a) Stress-strain response for the uniaxial testing specimens and b) bending check for all 6 specimens. The red line represents the tensile stiffness as measured in Ref. [7]. (For interpretation of the references to colour in this figure legend, the reader is referred to the Web version of this article.)

Table 2
Summary of the experimental results of the uniaxial testing specimens and comparison with the tensile data obtained in [7].

Testing	Strength (MPa)	Strain-to-failure (%)
Tension [7]	674 ± 49	0.96 ± 0.10
Compression (linear response)	−552 ± 55	−0.79 ± 0.08
Compression (all specimens)	−476 ± 88	−0.87 ± 0.10

3.2.1. *Damage characterisation*

Fig. 9 shows characteristic damage in the short and long SBB specimens. There was no debonding between the core and the top/bottom skins and no damage observed in these interfaces. Also, the areas where patches were used for the top skin beam extensions did not show any signs of damage. All specimens failed in the gauge section of the top skin (Fig. 9a) and no damage was observed in the PMMA core or the UD bottom skin. For some specimens the damage extended to the load application points and some delaminations within the TBDC were observed (Fig. 9b). However, the most common failure mode was clean

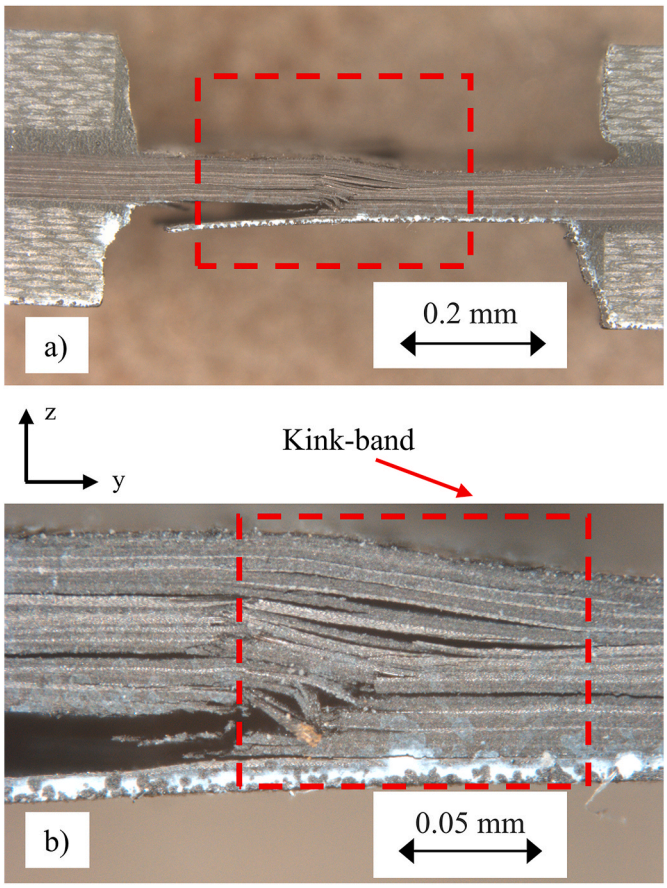

Fig. 7. Macroscopic view of a uniaxial testing specimen highlighting the a) misalignment developed due to buckling and b) the "macroscopic kind band".

single translaminar cracks in the top side of the TBDC skin at angles of about 15–45° to the normal to the loading direction (Fig. 9c). These observations are consistent with the damage observed in Ref. [21] for UD composites, and also in Ref. [17] for quasi-isotropic laminates; the lower range of angles observed here is consistent with typical kink-band angles reported for load-aligned plies, while the higher range is consistent with splitting of angle-plies, suggesting that the micro-mechanical damage mechanisms in TBDCs are influenced by the local orientation of the tows.

The measured compressive strains, which were equal or even exceeded the measured tensile strains, along with the macroscopic observations show that the specimens reached their compressive strength and did not fail prematurely. However, the fracture mechanism remained unclear, and SEM was utilised to study the fracture surfaces in more detail. Fig. 10 shows a general overview (Fig. 10a and d at ×500 magnification) of a characteristic fracture surface (from the areas close to the translaminar cracks) from the short (left) and long (right) SBB specimens. The general overview revealed the presence of shear cusps and fibre imprints which are consistent with matrix deformation at the tape interface level leading to tape shear-out. The tape shear-out is practically identical to the tape pull-out observed to occur during the static and fatigue tensile testing of the ultra-thin TBDCs [7,8].

However, Fig. 10 also revealed one additional feature that had not been observed in TBDC testing before. Large cracks, almost perpendicular to the fibre direction, extending through the width of the tapes were detected (Fig. 10a and d). Such cracks were observed in the literature for continuous composites and were described as gouges or ribs which typically occur at multidirectional interfaces [31]. The gouges are associated with shear fracture of the inter-ply (or in this context inter-tape) resin layer and typically form before the shear cusps develop,

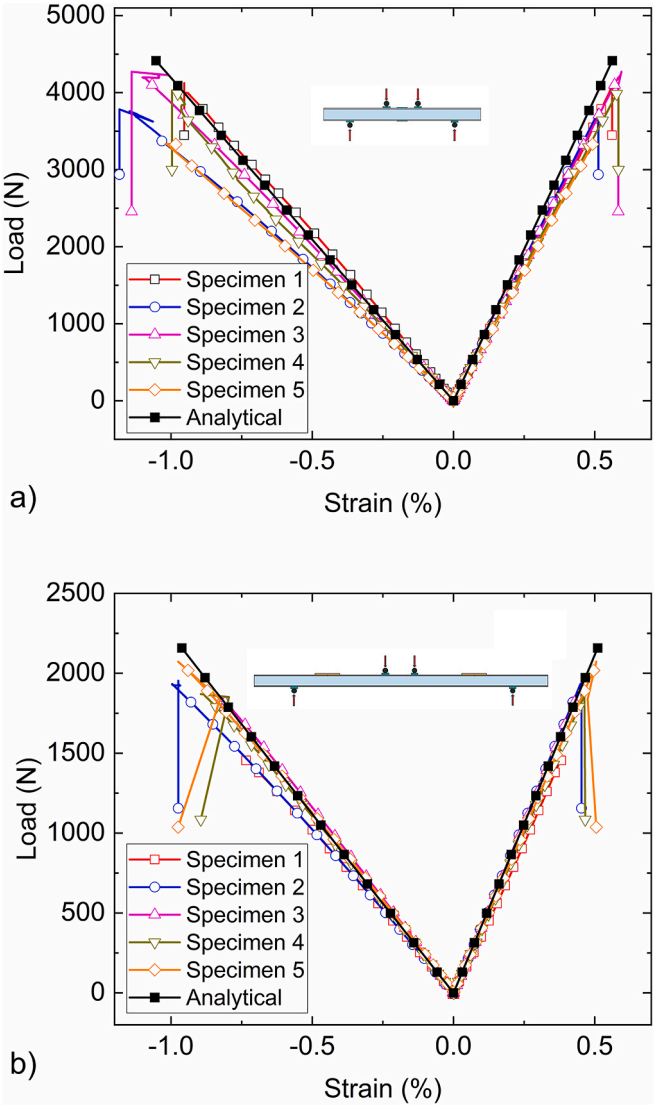

Fig. 8. Load strain response for the a) short and b) long SBB specimens, measured on the top TBDC skin (negative values) and at the bottom UD skin (positive values).

Table 3
Summary of the experimental results from the SBB testing and comparison with uniaxial compressive and tensile testing.

Testing	Strain-to-failure (%)	Strength (MPa)
SBB short	−1.05 ± 0.08	−735 (estimated)
SBB long	−0.96 ± 0.10	−674 (estimated)
Uniaxial compression	−0.79 ± 0.08	−552
Uniaxial tension	0.96 ± 0.10	674

which follow later as the delamination progresses. It should be noted that the gouges and the cusps are an effect of the same damage mechanism which is connected to tape shear-out due to deformation of the matrix at the tape interfaces. Fig. 10b–e shows a more detailed view of these cracks, and the discontinuities caused in the tapes. Additional matrix deformation can also be observed through the thickness of the gouges (Fig. 10c and f). The gouges were present in both the long and the short SBB specimens. However, it is worth noting that these features were more pronounced in the long SBB specimens as they were denser (Fig. 10a and c).

The tape shear-out highlights that the interfaces between the tapes

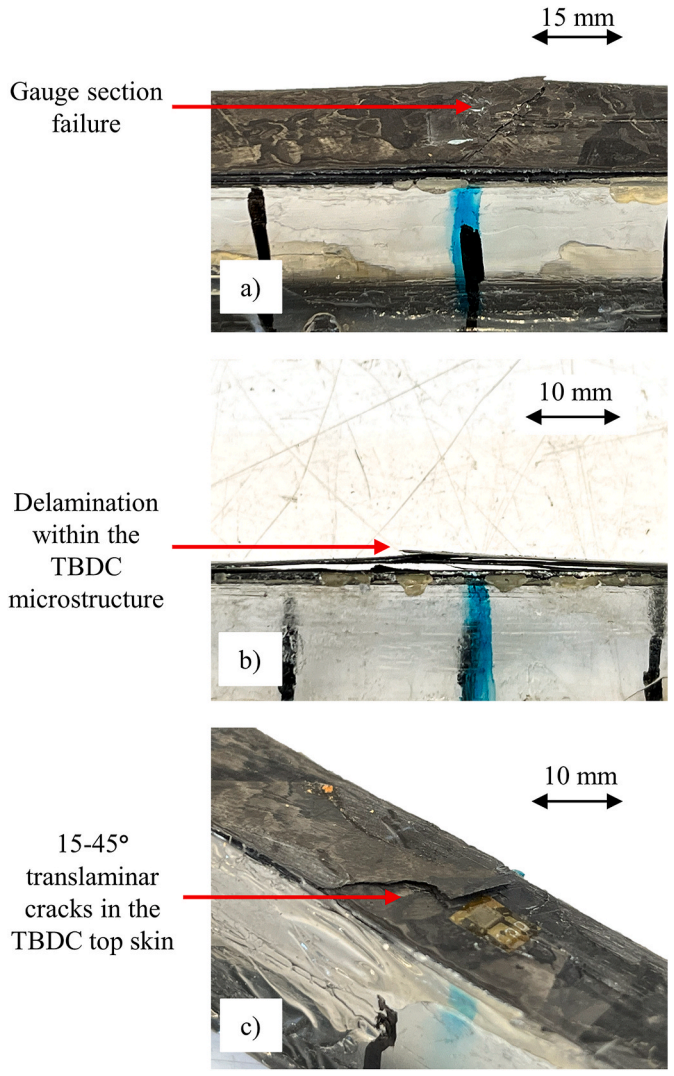

Fig. 9. Macroscopic failure for the SBB specimens highlighting a) the damage in the gauge section, b) the delaminations within the TBDC microstructure and c) the translaminar cracks forming in the TBDC top skin.

are relatively weak. More specifically, mode II fracture toughness was measured in previous publications [7] and the average value was around 500 J/m2 which is relatively low for the matrix systems typically used in high-performance composites. However, the low values of mode II fracture toughness are connected to the use of ultra-thin tapes, as there is not enough space for the resin to deform and dissipate more energy during fracture. Finally, it must be highlighted that there is no conclusive evidence regarding the sequence of damage (tape shear-out and translaminar cracks).

4. Discussion

In a previous publication [7], the authors developed an analytical framework which could predict the stiffness and strength of ultra-thin TBDCs under uniaxial tensile loading. There, three competing damage mechanisms were identified which related to longitudinal tape fracture, transverse tape fracture and tape pull-out. It was also shown that for this material system, tape pull-out was the most dominant damage mechanism. Under compressive loading, three damage mechanisms are also expected to compete. Firstly, the thin tapes can fail by fibre micro-buckling, i.e. kink-band formation. Secondly, the tapes can break transversely from the high compression load and finally, the tapes can fail by shearing-out (i.e. sliding against each other).

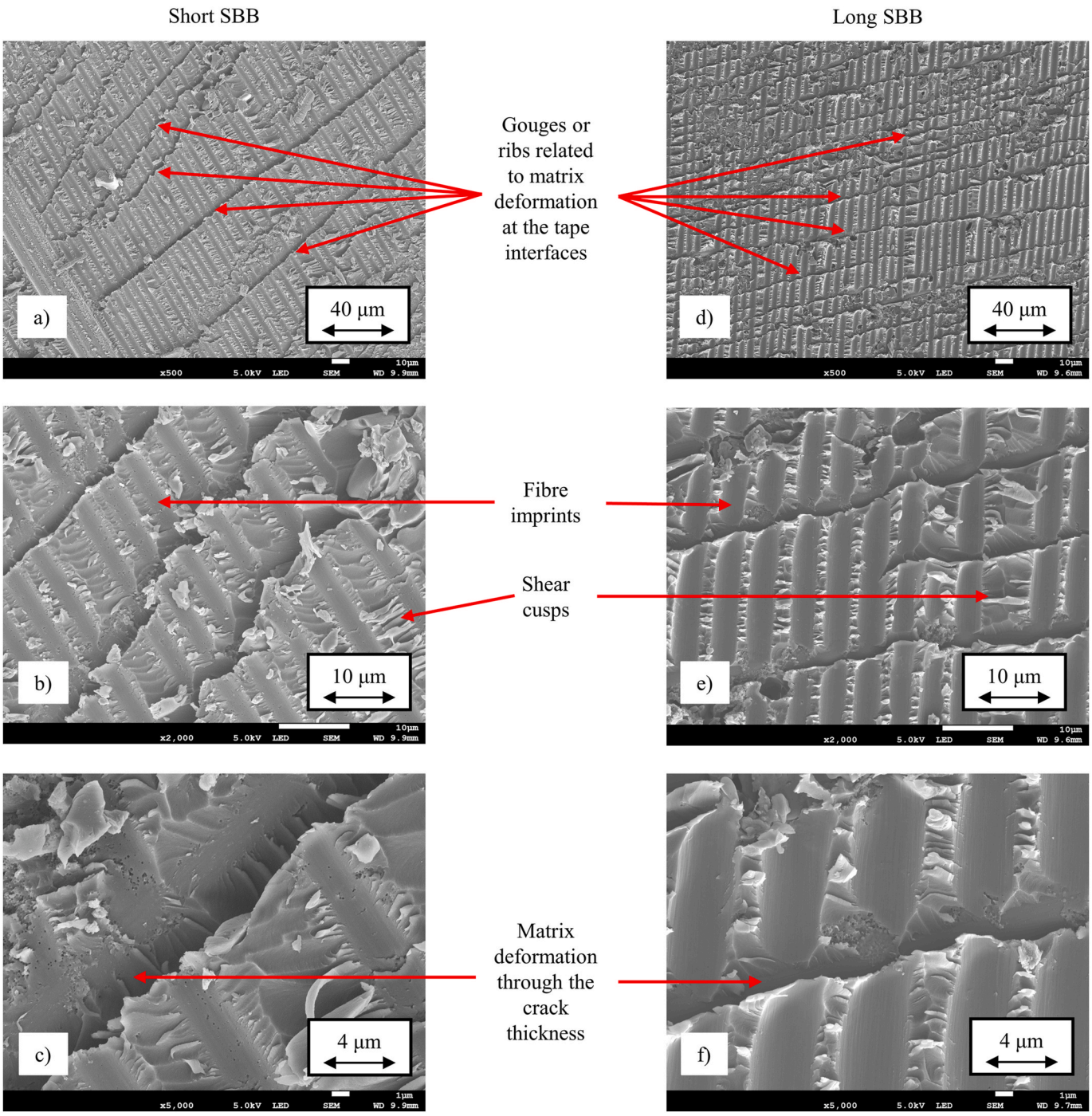

Fig. 10. SEM analysis on the TBDC top skin of the SBB specimen across different scales (x500, ×2000 and ×5000 magnification). The left side shows the short SBB fracture surfaces while the right side shows the long SBB fracture surfaces.

The SEM observations described in section 3.2.1 show that the compressive damage of the ultra-thin TBDCs was not controlled by instabilities and fibre kinking or transverse tape fracture but by matrix deformation at the tape interfaces. Therefore, the predictive tool developed for the tensile response of the ultra-thin TBDCs is expected to be valid under compressive loads as well. As a result, the compressive strain-to-failure of the ultra-thin TBDCs can be expressed as

$$\varepsilon_{compr} = \frac{1}{\overline{E}_x}\sqrt{\frac{2E_{tape(\theta)}G_{IIc}}{t_{tape}}} \tag{1}$$

In equation (1), $\overline{E}_x$ is the in-plane modulus of the composite, $E_{tape(\theta)}$ is the tape modulus as a function of the angle, G_{IIc} is the mode II interfacial fracture toughness and t_{tape} is the thickness of the tapes. The in-plane modulus can be calculated using the Equivalent Laminate (EL) theory [32] assuming an equivalent quasi-isotropic laminate with 8 total plies $[0,45,-45,90]_s$, while the tape modulus was calculated as a function of the tape angle and the elastic constants of the tapes. The in-plane modulus estimated using the EL theory also had excellent agreement with the experimental measurements during tensile testing [7]. Finally, the mode II interfacial fracture toughness was measured experimentally. Details for all calculations and measurements can be found in Katsivalis et al. [7].

Based on Equation (1), the predicted maximum compressive strain

was 0.87 % which is about 10 % lower compared to the measured values during the SBB test. The differences between the experimental and analytical methods could be connected to small differences in the fibre volume fractions which would influence the elastic constants in the laminates but also variations in the interlaminar shear fracture toughness. As shown in Equation (1), elevated values of mode II fracture toughness could increase the value of the shear-out strain significantly and thus activate competing damage mechanisms such as fibre kinking or fibre shear fracture. However, such observations were not made for this material system highlighting the beneficial effect of the ultra-thin tapes and the TBDC microstructure.

The compressive strains achieved with the SBB specimens reached or even exceeded the tensile response of the ultra-thin TBDCs. Similar observations were made in the past by authors working on TBDCs [2,23,24]. In these studies, it was concluded that the agreement between tensile and compressive strength is a result of the weaker tensile response. In fact, the tensile and compressive strengths reported in these studies did not exceed 300 MPa. In our study, the ultra-thin TBDCs are high-performance and reached a strength of about 700 MPa. The reason for the agreement between the tensile and the compressive strength is related to the TBDC microarchitecture which leads to similar damage mechanisms. More specifically, the ultra-thin tapes practically eliminate longitudinal and transverse tape fractures and instabilities but promote tape pull-out and shear-out at higher strain levels.

The results displayed in this study for the ultra-thin TBDCs are directly comparable and in some cases even exceed the compressive strength reported in the literature for ordinary QI laminates [17,33–36]. The improved mechanical response combined with the increased manufacturability, the improved forming capabilities and the minimised scrap and waste material highlight the superiority of well-designed ultra-thin TBDCs when compared to conventional QI laminates.

5. Conclusions

An experimental campaign consisting of two different test setups was conducted to extract the properties of ultra-thin TBDCs under compressive loading. The first test setup was based on uniaxial testing while the second test setup was based on a sandwich beam bending specimen. The compressive damage was studied using SEM images while an analytical model was used which provided insights into the performance of the SBB specimens.

The uniaxial testing of the TBDCs led to bending and premature failures in all specimens. More specifically, three specimens displayed an initially linear stress-strain response (following the tensile stiffness of the ultra-thin TBDCs) before failing at about 80 % of the tensile strength of the material. The remaining three specimens displayed highly nonlinear response even at low loads. Analysis of the failed specimens showed clear misalignments and the forming of macroscopic kink bands. This highlights the limitations of uniaxial testing for high-performance ultra-thin TBDCs.

The SBB testing allowed to explore the full potential of TBDCs under compressive loading. More specifically, the compressive strains measured during the SBB tests reached (long SBB) or exceeded (short SBB) the tensile strain-to-failure of the ultra-thin TBDC material. The compressive strain-to-failure measured during the SBB testing exceeded 1 % which was an about 20 % increase compared to the values recorded during uniaxial compression.

The elevated compressive properties are a result of the TBDC microstructure which meant that failure did not occur due to instability development. Instead, the damage mechanism was controlled by matrix deformation in the tow interfaces which eventually led to tape shear-out. This was confirmed by two distinct damage features in the SEM analysis, the presence of shear cusps and gouges. These findings were similar to the damage mechanisms under uniaxial loading and thus explain the close agreement between the tensile and compressive properties. Therefore, the analytical approach developed for the prediction of uniaxial tensile strength was considered to be valid under uniaxial compression and underpredicted the compressive strain-to-failure by about 10 %.

The compressive strength of composites has traditionally been very complex to measure accurately but also a limiting parameter in the design of composite structures. This paper demonstrates that the SBB test produced consistent and repeatable compressive damage at high levels of strain. In addition, it was shown that the compressive strength of ultra-thin TBDCs is equal to their tensile strength and could even outperform conventional continuous QI laminates. It is evident that the contribution of this paper is not limited to addressing testing issues but provides an understanding in the complex performance of ultra-thin TBDCs under compressive loads by performing a detailed analysis of the observed damage and failure mechanisms. This highlights the potential of using ultra-thin TBDCs in demanding structural applications. An important step in building more confidence in this new material concept would be the development of accurate numerical methods for the stiffness and strength prediction of ultra-thin TBDCs. In addition, the experimental characterisation needs to be expanded to more complex load cases such as notched behaviour and performance under environmental exposure.

CRediT authorship contribution statement

Ioannis Katsivalis: Writing – original draft, Software, Methodology, Investigation, Formal analysis, Data curation, Conceptualization. **Aree Tongloet:** Writing – review & editing, Methodology, Investigation. **Xun Wu:** Writing – review & editing, Methodology, Investigation. **Monica Norrby:** Writing – review & editing, Investigation. **Florence Moreau:** Writing – review & editing, Resources. **Soraia Pimenta:** Writing – review & editing, Methodology, Investigation, Funding acquisition, Formal analysis, Conceptualization. **Michael R. Wisnom:** Writing – review & editing, Methodology, Investigation, Funding acquisition, Formal analysis, Conceptualization. **Dan Zenkert:** Writing – review & editing, Methodology, Investigation, Funding acquisition, Formal analysis, Conceptualization. **Leif E. Asp:** Writing – review & editing, Methodology, Investigation, Funding acquisition, Formal analysis, Conceptualization.

Declaration of competing interest

The authors declare that they have no known competing financial interests or personal relationships that could have appeared to influence the work reported in this paper.

Acknowledgements

The authors would like to acknowledge funding from VINNOVA (The Swedish Innovation Agency) for the Fatresfeet project (dnr. 2021–04048) and the Swedish Energy Agency via its Competence Centre Technologies and innovations for a future sustainable hydrogen economy (TechForH2, dnr. 2021–036176). The Competence Centre TechForH2 is hosted by Chalmers University of Technology and is financially supported by the Swedish Energy agency (P2021 - 90268) and the member companies Volvo, Scania, Siemens Energy, GKN Aerospace, PowerCell, Oxeon, RISE, Stena Rederier AB, Johnson Matthey and Insplorion. The authors would also like to acknowledge the strategic innovation program LIGHTer (funding provided by Vinnova, the Swedish Energy Agency and Formas).

Data availability

Data will be made available on request.

References

[1] Wan Y, Takahashi J. Tensile and compressive properties of chopped carbon fiber tapes reinforced thermoplastics with different fiber lengths and molding pressures. Compos Appl Sci Manuf 2016;87:271–81.
[2] Martulli LM, Muyshondt L, Kerschbaum M, Pimenta S, Lomov SV, Swolfs Y. Carbon fibre sheet moulding compounds with high in-mould flow: linking morphology to tensile and compressive properties. Compos Appl Sci Manuf 2019;126:105600.
[3] Alves M, Li Y, Pimenta S. Spatial variability and characteristic length-scales of strain fields in tow-based discontinuous composites: characterisation and modelling. Compos B Eng 2023;262:110789.
[4] Gulfo L, Haglund Nilsson O, Sjöberg J, Katsivalis I, Asp LE, Fagerström M. A 3D voxel-based mesostructure generator for finite element modelling of tow-based discontinuous composites. Compos B Eng 2024;278:111405.
[5] Jackson AP, Vincent Julian FV, Turner RM. The mechanical design of nacre. Proc R Soc Lond B Biol Sci 1988;234:415–40.
[6] Askarinejad S, Wang S, Shalchy F, Rosewitz J, Choshali HA, Rahbar N. Deformation and toughening mechanisms in nacreous structures, reference module in materials science and materials engineering. Elsevier; 2022.
[7] Katsivalis I, Persson M, Johansen M, Moreau F, Kullgren E, Norrby M, Zenkert D, Pimenta S, Asp LE. Strength analysis and failure prediction of thin tow-based discontinuous composites. Compos Sci Technol 2024;245:110342.
[8] Katsivalis I, Norrby M, Moreau F, Kullgren E, Pimenta S, Zenkert D, Asp LE. Fatigue performance and damage characterisation of ultra-thin tow-based discontinuous tape composites. Compos B Eng 2024;281:111553.
[9] Alves M, Carlstedt D, Ohlsson F, Asp LE, Pimenta S. Ultra-strong and stiff randomly-oriented discontinuous composites: closing the gap to quasi-isotropic continuous-fibre laminates. Compos Appl Sci Manuf 2020;132.
[10] Camanho PP, Dávila CG, Pinho ST, Iannucci L, Robinson P. Prediction of in situ strengths and matrix cracking in composites under transverse tension and in-plane shear. Compos Appl Sci Manuf 2006;37:165–76.
[11] Budiansky B, Fleck NA. Compressive failure of fibre composites. J Mech Phys Solid 1993;41:183–211.
[12] Tanaka F, Okabe T, Okuda H, Kinloch IA, Young RJ. The effect of nanostructure upon the compressive strength of carbon fibres. J Mater Sci 2013;48:2104–10.
[13] Fleck NA, Budiansky B. Compressive failure of fibre composites due to microbuckling. In: Dvorak GJ, editor. Inelastic deformation of composite materials. New York, NY: Springer New York; 1991. p. 235–73.
[14] Berbinau P, Soutis C, Guz IA. Compressive failure of 0° unidirectional carbon-fibre-reinforced plastic (CFRP) laminates by fibre microbuckling. Compos Sci Technol 1999;59:1451–5.
[15] ASTM, D3410/D3410M. Standard test method for compressive properties of polymer matrix composite materials with unsupported gage section by shear loading. West Conshohocken, PA: ASTM International; 2021.
[16] Jelf PM, Fleck NA. The failure of composite tubes due to combined compression and torsion. J Mater Sci 1994;29:3080–4.
[17] Lee J, Soutis C. A study on the compressive strength of thick carbon fibre–epoxy laminates. Compos Sci Technol 2007;67:2015–26.
[18] Wisnom MR, Atkinson JW, Jones MI. Reduction in compressive strain to failure with increasing specimen size in pin-ended buckling tests. Compos Sci Technol 1997;57:1303–8.
[19] Yokozeki T, Ogasawara T, Ishikawa T. Evaluation of compressive nonlinear response of unidirectional carbon fiber reinforced composites using a modified sandwich beam specimen in flexure. J Reinforc Plast Compos 2008;27:5–17.
[20] Yokozeki T, Ogasawara T, Ishikawa T. Nonlinear behavior and compressive strength of unidirectional and multidirectional carbon fiber composite laminates. Compos Appl Sci Manuf 2006;37:2069–79.
[21] Wu X, Wisnom MR. Compressive failure strain of unidirectional carbon fibre composites from bending tests. Compos Struct 2023;304:116467.
[22] ASTM, ASTM D5467/D5467M-97. Standard test method for compressive properties of unidirectional polymer matrix composite materials using a sandwich beam. West Conshohocken, PA: ASTM International; 2017. 2017.
[23] Feraboli P, Peitso E, Deleo F, Cleveland T, Stickler PB. Characterization of prepreg-based discontinuous carbon fiber/epoxy systems. J Reinforc Plast Compos 2008;28:1191–214.
[24] Selezneva M, Lessard L. Characterization of mechanical properties of randomly oriented strand thermoplastic composites. J Compos Mater 2015;50:2833–51.
[25] Martulli LM, Muyshondt L, Kerschbaum M, Pimenta S, Lomov SV, Swolfs Y. Morphology-induced fatigue crack arresting in carbon fibre sheet moulding compounds. Int J Fatig 2020;134:105510.
[26] Wilhelmsson D, Talreja R, Gutkin R, Asp LE. Compressive strength assessment of fibre composites based on a defect severity model. Compos Sci Technol 2019;181:107685.
[27] Huntsman, araldite 2022-1 technical datasheet, basel. 2019.
[28] Hexcel. HexTow® IM7 carbon fiber - product. Data Sheet; 2023.
[29] Perspex. Perspex® cell cast acrylic - product data sheet. 2023.
[30] Zenkert D. An introduction to sandwich structures. 1995. Stockholm.
[31] Greenhalgh ES. 4 - delamination-dominated failures in polymer composites. In: Greenhalgh ES, editor. Failure analysis and fractography of polymer composites. Woodhead Publishing; 2009. p. 164–237.
[32] Li Y, Pimenta S, Singgih J, Nothdurfter S, Schuffenhauer K. Experimental investigation of randomly-oriented tow-based discontinuous composites and their equivalent laminates. Compos Appl Sci Manuf 2017;102:64–75.
[33] Wang J, Callus PJ, Bannister MK. Experimental and numerical investigation of the tension and compression strength of un-notched and notched quasi-isotropic laminates. Compos Struct 2004;64:297–306.
[34] Goto K, Arai M, Kano Y, Hara E, Ishikawa T. Compressive fracture aspect of thick quasi-isotropic carbon fiber reinforced plastic laminates. Compos Sci Technol 2019;181:107706.
[35] Gao Y, Wang J, Song X, Ding H, Wang H, Bi Y, Ke Y. Investigation on the compressive mechanical properties of ultra-thick CFRP laminates. Int J Mech Sci 2023;241:107966.
[36] Ogasawara T, Mikami T, Takamoto K, Asakawa K, Aoki K, Uchiyama S, Sugimoto S, Yokozeki T. Experimental evaluation of filled-hole compressive strengths of thin-ply carbon fiber/epoxy composite laminates. Compos Sci Technol 2023;237:109996.